Available online at www.sciencedirect.com

SCIENCE DIRECT®

Tectonophysics 405 (2005) 47–63

TECTONOPHYSICS

www.elsevier.com/locate/tecto

Mesozoic lithospheric deformation in the North China block: Numerical simulation of evolution from orogenic belt to extensional basin system

Yanghua Wang [a,*], G.A. Houseman [b], G. Lin [c], F. Guo [c], Y.-J. Wang [c], W.-M. Fan [c], X. Chang [d]

[a] *Imperial College London, Centre for Reservoir Geophysics, Department of Earth Science and Engineering, Prince Consort Road, London SW7 2BP, UK*
[b] *University of Leeds, School of Earth and Environment, Leeds LS2 9JT, UK*
[c] *Chinese Academy of Sciences, Guangzhou Institute of Geochemistry, Wushan, Guangzhou 510640, China*
[d] *Chinese Academy of Sciences, Institute of Geology and Geophysics, Beijing 100029, China*

Received 15 October 2003; accepted 12 May 2005
Available online 11 July 2005

Abstract

Horizontal extension of a previously thickened crust could be the principal mechanism that caused the development of widespread extensional basins throughout the North China block (Hua-Bei region) during the Mesozoic. We develop here a regional tectonic model for the evolution of the lithosphere in the North China block, based on thin sheet models of lithospheric deformation, with numerical solutions obtained using the finite element method. The tectonic evolution of this region is defined conceptually by two stages in our simplified tectonic model: the first stage is dominated by N–S shortening, and the second by E–W extension. We associate the N–S shortening with the Triassic continental collision between the North and South China blocks, assuming that the Tan-Lu Fault system defines the eastern boundary of the North China block. The late Mesozoic E–W extension that created the Mesozoic basin systems requires a change in the regional stress state that could have been triggered by either or both of the following factors: First, gravitational instability of the lithosphere triggered by crustal convergence might have removed the lower layers of the thickened mantle lithosphere and thus caused a rapid increase in the local gravitational potential energy of the lithosphere. Secondly, a change to the constraining stress on the eastern boundary of the North China block, that might have been caused by roll-back of the subducting Pacific slab, could have reduced the E–W horizontal stress enough to activate extension. Our simulations show that widespread thickening of the North China block by as much as 50% can be explained by the collision with South China in the Triassic and Jurassic. If convergence then ceases, E–W extension can occur in the model if the eastern boundary of the region can move outwards. We find that such extension may occur, restoring crustal thickness of order 30 km within a period of 50 Myr or less, if the depth-averaged constitutive relation of the lithosphere is Newtonian, and if the Argand number (the ratio of buoyancy-derived stress to viscous stress) is greater than

* Corresponding author.
E-mail address: yanghua.wang@imperial.ac.uk (Y. Wang).

0040-1951/$ - see front matter
doi:10.1016/j.tecto.2005.05.012

about 4. Widespread convective thinning of the lithosphere is not required in order to drive the extension with these parameters. If, however, the lithospheric viscosity is non-Newtonian (with strain-rate proportional to the third power of stress) the extensional phase would not occur in a geologically plausible time unless the Argand number were significantly increased by a lithospheric thinning event that was triggered by crustal thickening ratios as low as 1.5.

Keywords: Basin formation; Continental shortening and extension; Crustal deformation; Geodynamics; North China block; Thin sheet models; Lithospheric thinning

1. Introduction

The North China block, the western portion of the Sino-Korean Craton, is bounded to the north by the Yanshanian orogenic belt and to the south by the Qinling-Dabie orogenic belt (Fig. 1). Şengör and Natal'in (1996) describe the northern boundary of the North China block as comprised of displaced fragments of the active margin of the North China craton, including medial to late Paleozoic subduction-accretion complexes and related magmatic arcs. The collision between the North China/Tarim block and the Altaid system of Mongolia began in the late Carboniferous (Yin and Nie, 1996). On its southern boundary the North China block is separated from South China by the Qinling-Dabie-Sulu suture zone, which extends westward to the Kunlun Shan. During the late Permian, South China began colliding with North China, initially in the East, but the collision progressively migrated westward along this suture zone (Yin and Nie, 1996).

The North China basement includes Archean age rocks and widespread Proterozoic sedimentary cover. During the Paleozoic, the North China block was a stable craton with shallow marine carbonate sedimentation, giving way in the Carboniferous to terrestrial deposition (Yin and Nie, 1996). Intracontinental deformation was widespread in both South and North China in the Mesozoic. The structures relating to the Yanshanian orogeny (late Jurassic to early Cretaceous) are characterized by E–W trending folds and thrusts in the northern part of North China. Evidence

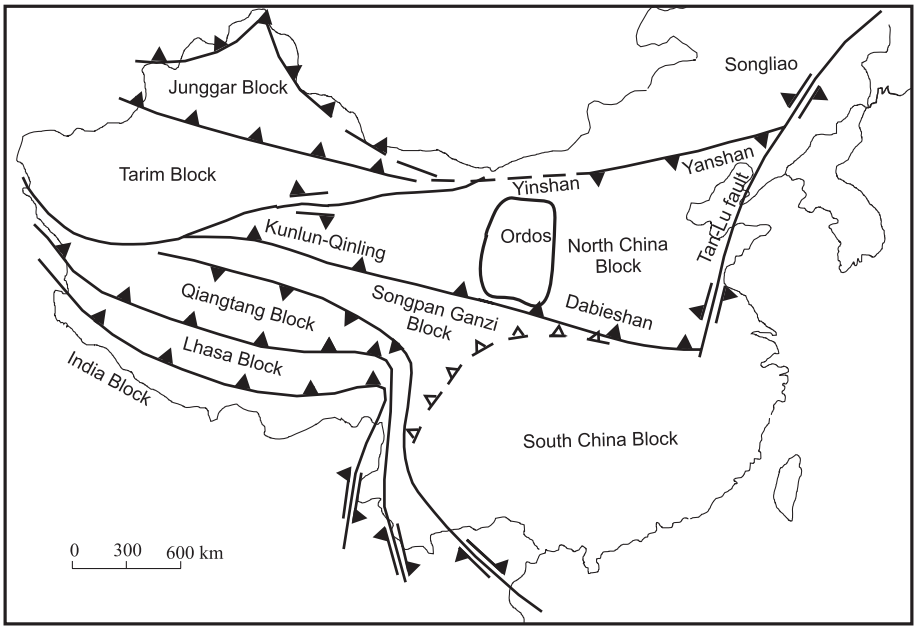

Fig. 1. Tectonic sketch map of China, showing the location of North China block (Hua-Bei region) and of major suture zones.

of ductile shear zones formed at 211 Ma and subsequently cut by brittle thrust systems is preserved (Hacker et al., 2000; Ratschbacher et al., 2000). The late Jurassic E–W trending fold and thrust belt can be traced from the Liaoning region to the eastern Tien Shan and indicates clearly that N–S shortening occurred in the North China block. In the Dabie orogenic belt, ductile shear zones were formed during the Triassic with north-verging thrusts of the mid-late Jurassic switching to south-verging in the late Jurassic–early Cretaceous (Wang et al., 1996; Hacker et al., 2000; Liu et al., 2003). The Triassic continental collision between the North and South China blocks may be considered as a driving force for north–south shortening in the Yanshanian, although subduction zones to the east and north may also have played a role.

The Tan-Lu Fault is a major structure forming the present-day eastern boundary of the North China block (Fig. 2), though Korean basement to the east is clearly correlated with that of the North China block, with the whole often referred to as the Sino-Korean platform. Diabases erupted at 103 Ma postdate initial movement on the fault. Sinistral slip is documented in the mid Cretaceous at ~100–97.5 Ma whereas dextral movement is indicated in the Tertiary (at ~63.5–45 Ma) (Xu et al., 1987; Zhu et al., 2001). The apparently large lateral offset of the ultra-high pressure rocks of Sulu and Dabie Shan regions was produced by that earlier phase of sinistral movement.

North–South contractional deformation of the North China block during the Triassic and early Jurassic evolved in the mid-late Jurassic to NE directed contraction (Davis et al., 2001), indicating perhaps that horizontal compressive stress on the southern boundary of the North China block was balanced against compressive stress on both northern and eastern boundaries. The NE directed contraction was both spatially and temporally associated with the emplacement of plutons and was followed in many places by E–W extension that continued through the Cretaceous. The widespread development of extensional basins in the Mesozoic of North China suggests extensional thinning of a previously thickened, unstable crust.

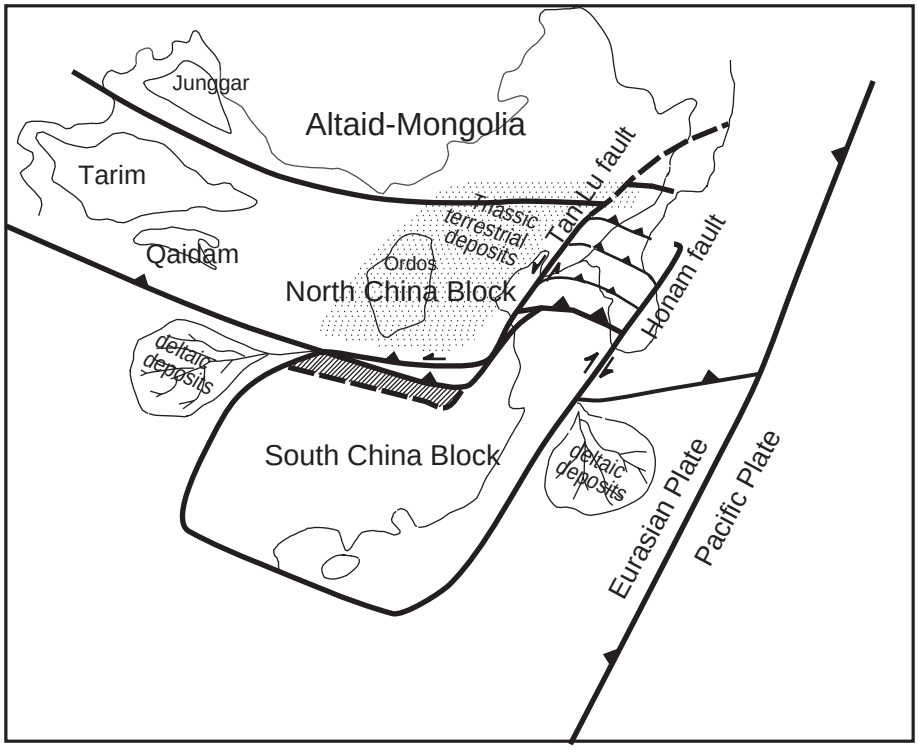

Fig. 2. The Triassic continental collision between the North and South China blocks (after Yin and Nie, 1993, 1996).

The implied lithospheric thinning is consistent with widely distributed basaltic magmatism (Menzies et al., 1993; Menzies and Xu, 1998; Fan et al., 2000) in the North China block during the late Mesozoic. During this period ductile shearing played an important role in the exhumation of high-grade metamorphics from the mid-lower crust. Basic and ultrabasic magmatism at this time is clearly related to the extensional structures. The cause of E–W directed lithospheric extension in the Cretaceous North China block is not clear, though the extensional collapse of crust thickened in the previous phase of N–S shortening may have provided the driving force. Slab roll-back of the westward subducting Pacific plate may also have provided an important boundary condition, necessary for extension to be triggered.

In this paper we develop a conceptual model of the two-stage history of the North China block as summarized above. We use the thin sheet model (Bird and Piper, 1980; England and McKenzie, 1982; England et al., 1985) to describe the horizontal distribution of lithospheric deformation in a numerical simulation of the Mesozoic development of the North China block. We use the finite element method (Houseman and England, 1986b, 1996) to solve the thin sheet stress-balance equations in order to obtain the distribution of strain-rate at a given time within the deforming block. The deformation geometry of this system is then computed by integrating the displacement-rate fields forward in time. In the first stage of this calculation we represent the effect of NS shortening during the Triassic and Jurassic. In this model we focus on the internal deformation of the North China block and do not explicitly represent the Qinling-Dabie suture zone and its associated deformation. By changing the boundary conditions on the thin viscous sheet for the second stage of the calculation, we then represent the EW extension of the Cretaceous.

We explore the hypothesis that the late Mesozoic extension episode is triggered by two factors: firstly a lithospheric thinning event consequent on crustal convergence which produced a sudden large increase in the local gravitational potential energy of the lithosphere (Houseman and England, 1986a; England and Houseman, 1989; Houseman, 1996), and secondly a change to the confining stress on the eastern boundary of the North China block, as might be caused by roll-back of the subducting Pacific slab. We treat the Tan-Lu Fault here as an eastern boundary for the Hua-Bei region in this tectonic model, though extension was presumably occurring also to the east of the Tan-Lu Fault, later developing the Bo-Hai Bay (Davis et al., 1996). The stress-state in this region is ultimately controlled by subduction occurring further to the East. We assume that, in the first stage of N–S convergence, this region to the east of the Tan-Lu Fault (Fig. 2) acted as a rigid constraint to eastward movement of the North China block. We relax this constraint in the second stage of the model deformation in order to simulate the effect of an extensional regime on this boundary induced by rollback of the subducting Pacific slab further to the east.

2. Numerical simulation

2.1. Governing equations

The general constitutive equation representing the ductile deformation of a thin non-Newtonian viscous sheet is given as

$$\bar{\tau}_{ij} = B\dot{E}^{(1/n)-1}\dot{\varepsilon}_{ij}, \tag{1}$$

where $\bar{\tau}_{ij}$ are the elements of the depth-averaged deviatoric stress tensor, $\dot{\varepsilon}_{ij}$ are elements of the strain-rate tensor (assumed independent of depth), $\dot{E}$ is the second invariant of the strain-rate tensor, n is the rheological exponent and B is a material constant which represents the strength of the lithosphfsere (England and McKenzie, 1982). If the material has a Newtonian viscosity ($n=1$), the strength parameter $B(x,y)$ is simply related to the depth-averaged viscosity $\eta(x,y)$ by $B=2\eta$.

The strain-rate components $\dot{\varepsilon}_{ij}$ are defined in terms of a continuum velocity distribution as

$$\dot{\varepsilon}_{ij} = \frac{1}{2}\left(\frac{\partial u_i}{\partial x_j} + \frac{\partial u_j}{\partial x_i}\right), \tag{2}$$

where u_i are horizontal velocity components, assumed invariant with depth in the thin viscous sheet.

The depth-averaged deviatoric stress components $\bar{\tau}_{ji}$ in the horizontal plane satisfy the following dimensionless equation

$$\frac{\partial \bar{\tau}_{ji}}{\partial x_j} - \frac{\partial \bar{\tau}_{zz}}{\partial x_i} = \frac{1}{2}\frac{\partial}{\partial x_i}\left(ArS^2\right), \tag{3}$$

where Ar is the Argand number, and S is the crustal to lithospheric thickness ratio. For a uniform crust of density ρ_c, overlaying a uniform mantle of density ρ_m, the Argand number is (England and McKenzie, 1982):

$$Ar = \frac{g\rho_c(1-\rho_c/\rho_m)L}{B(u_o/L)^{1/n}}, \quad (4)$$

where g is the gravitational acceleration, u_o is a displacement rate representative of the convergence velocity, and L is the thickness of a reference lithospheric column. The physical interpretation of the Argand number (England and McKenzie, 1982) is the ratio of the vertically averaged deviatoric stress associated with a crustal thickness contrast of order L to the stress required to deform the lithosphere at a characteristic strain rate $\dot{\varepsilon}_o = u_o/L$. The Argand number defined in (4) assumes isostatic balance with a compensation depth of L.

The evolution of crustal thickness can be obtained from the continuity equation (England and McKenzie, 1982):

$$\frac{1}{S}\frac{\partial S}{\partial t} = \dot{\varepsilon}_{zz} = -\left(\frac{\partial u_x}{\partial x} + \frac{\partial u_y}{\partial y}\right). \quad (5)$$

An implicit finite-difference representation (second order accurate) of the time derivative is used to advance the crustal thickness $S(x,y)$ from one time level to the next, and to simultaneously displace material points in the sheet to new locations. In the absence of information to the contrary, we assume an initial constant crustal thickness and an external geometry for the solution region as specified below.

Both for solving the equations and for describing the results in a physically objective way the equations are non-dimensionalized, following Houseman and England (1996). A length scale D=400 km based on the maximum convergent displacement of the southern boundary during the first stage of deformation, and a time scale T=100 Myr based on the duration of the deformation were used to render distance and time dimensionless, with the velocity scale defined accordingly:

$$u_o = \frac{D}{T} = 4\text{mm/year}. \quad (6)$$

The Argand number here is treated as an unknown variable, but its interpretation depends also on the ratio of horizontal length scale to vertical thickness of the lithosphere D/L, for which we assumed L=100 km, and on the initial crustal thickness, for which we assumed S_o=35 km. In the experiments described below, we consider values of n=1 and n=3, for the rheological exponent. England and Houseman (1986) determined that n=3 is about the minimum value for which plausible finite deformation models of the Cenozoic Indian-Asian continental collision can be constructed, but we also consider n=1 for comparison purposes. An exponent of n=3 is consistent with olivine deforming by dislocation creep, whereas n=1 is consistent with diffusion creep. The latter is more likely to dominate under high temperature-low stress conditions (Karato et al., 1986).

We assume here that the geodynamical evolution of the North China block in the Mesozoic may be adequately represented by two discrete phases of deformation, each constrained by a simple set of boundary conditions. The first stage represents the dominant N–S shortening during the Triassic and Jurassic (~250–150 Ma), and the second stage describes the E–W extension of the Cretaceous (~150–65 Ma). The time intervals of tectonic activity are not precisely constrained but are roughly linked to the Triassic–Jurassic collisional event between North and South China blocks (with dates for example of 224 Ma, Li et al., 1993; 244 Ma, Zheng et al., 2002), and the early Cretaceous age of emplacement of voluminous mafic magmas dated for example at 128 Ma (Guo et al., 2003) and mylonites dated at 130–128 Ma using the Ar–Ar technique (Zhu et al., 2001). We also recognise that deformation that occurred during these periods may have occurred at variable rates or even episodically rather than at the continuous strain rates implied by our simplified parameterisation.

2.2. Tectonic model—stage 1

Our numerical simulations are based on Yin and Nie's (1993, 1996) model of the collision and tectonic evolution of South and North China blocks. This tectonic model, redrawn in Fig. 2, may be summarized as follows:

1. The southern margin of the North China block was a relatively straight, northward dipping subduction

zone. Prior to the collision, the northern margin of the South China block was irregular, extending 550 km further to the north in the Hua-dong/Huang-hai region east of the Tan-Lu Fault. The collision of South and North China blocks started in late Permian in that region between the Tan-Lu fault and the Honam shear zone (Fig. 2) with the indentation of the northeastern part of the South China block. Thrusts, folds, and related foreland basins developed near the collision zone, accompanied by near continuous volcanism. Sediments eroded from the collision zone represented by the Qinling-Dabie orogen were deposited in foreland basins on both Yangtze craton to the South and Sino-Korean craton to the North.

2. Due to the irregularity of the northern margin of the South China block, the ocean in the eastern part of the future Dabie belt closed first during the early to middle Triassic. In response to this diachronous closure of the ocean, volcanism related to subduction had systematically shut down westward from the Tan-Lu Fault along the Dabie suture zone. During the Triassic, sediments derived from the Dabie Shan and Shandong regions were deposited in the Songpan-Ganzi Complex to the south of the Qinling-Dabie belt, an area which has been interpreted as a Triassic remnant ocean basin (Zhou and Graham, 1996). A consequence of the N–S crustal shortening in an extensive region of North China during the Triassic was the formation of a topographically elevated region, the Hua-bei Plateau, which received little Triassic clastic sedimentation.
3. During the Jurassic, sinistral motion on the Tan-Lu fault continued, with ongoing convergence between North and South China blocks. The late Jurassic E–W trending Qinling-Dabie fold belt could be traced from Liaoning in the East to the Tarim Basin in the west. The northern margin of the North China (Hua-Bei) block is marked by the fold belts of the Yan Shan in east China and its lateral equivalent to the west, the Yin Shan. The environment of N–S convergence associated with the Yanshanian orogeny has also been attributed (in part perhaps) to subduction of the Mongol-Okhotsk plate beneath North China and to the collision of the Lhasa block with Eurasia in the South.

For the numerical simulation we define a polygonal solution region representing the North China block, based on Yin and Nie's (1993, 1996) summary of the collision and tectonic evolution of this region. Our representation of the solution region at time zero (Fig. 3) shows the North China block at the beginning of the collision. In this and subsequent diagrams, the solution is shown in normal map orientation with x and y directions corresponding approximately to E and N. Overall rotation of the model is not constrained however, and the final model requires a clockwise rotation on the order of 30° for comparison with actual geology. Distances are labelled in dimensionless length units described above, relative to an arbitrary stationary origin in the SW corner of the solution region. With a length unit of $D=400$ km, the rigid western boundary is 1000 km long and the northern boundary is initially 2400 km long.

The solution of the thin sheet equations requires boundary conditions on both components of either displacement rate (u_x, u_y) or traction (T_x, T_y). The boundary conditions used in the first stage of the numerical simulation are as follows:

The northern ($y=2.5$) and western ($x=0$) boundaries are rigid:

$$u_x = 0, \qquad u_y = 0; \tag{7}$$

The eastern ($x=6$) boundary representing the Tan-Lu Fault is here assumed to act as a sliding boundary, assuming that the west Pacific subduction zone has not yet begun to affect the development of this region:

$$u_x = 0, \qquad T_y = 0, \tag{8}$$

and convergence on the southern boundary (initially $y=-x/12$) is driven by a northward displacement rate that increases from 0 at the SW corner to 1 (dimensionless) at the SE corner:

$$T_x = 0, \qquad u_y = \frac{x}{6}. \tag{9}$$

The actual history of convergence in this case is poorly constrained. Although the total duration of convergence suggests an average convergence rate of 4 mm/year, convergence rates may have been intermittently higher. By comparison the modern-day convergence rate between India and Asia is on

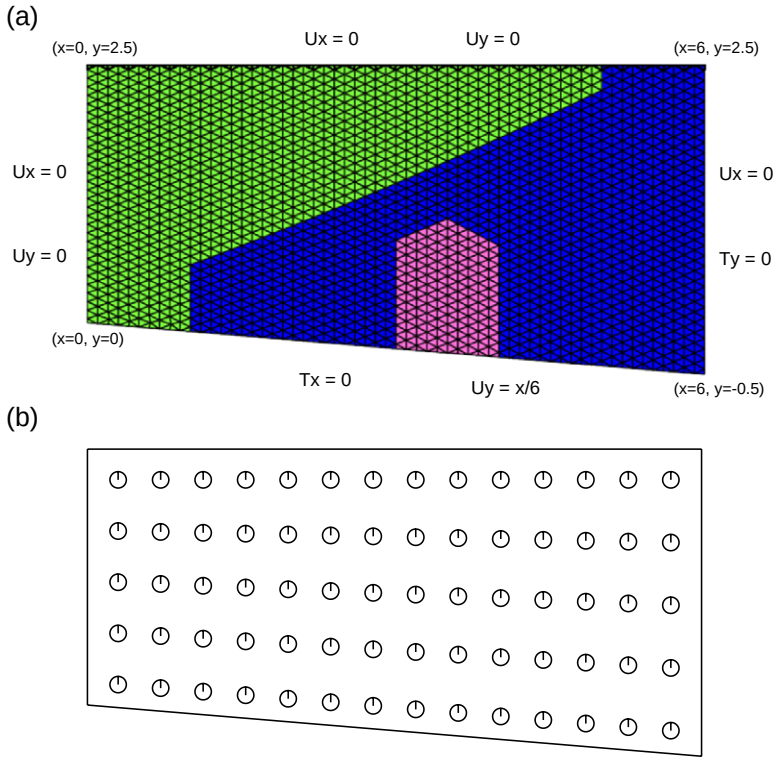

Fig. 3. (a) Finite element discretization of the solution region, and specification of the boundary conditions used in Stage 1 of the numerical experiments. For simplicity we refer to the x-direction as East and the y-direction as North. The small light-coloured region represents the Ordos block; it is surrounded by the relatively weak North China block, with the stronger Altaid-Mongolia region to the northwest. (b) Initially circular strain markers are distributed across the region for visualization of local strain.

the order of 50 mm/year. The eastward increasing convergence rate represents the idea (Yin and Nie, 1993, 1996) that the collision started first in Shandong (east) during the early Permian and propagated westward to the Dabie region in the middle to the late Triassic and to the Qinling region in the late Triassic to early Jurassic.

2.3. Tectonic model—Stage 2

Early Cretaceous E–W extension occurred in southern Liaoning and the Hua-Bei region, contemporaneous with NE–SW extension in western Inner Mongolia (Zheng et al., 2001). That extensional event marked the collapse of the Hua-Bei plateau to become the Hua-Bei Basin, bounded on the west by the Ordos and on the east by the Tan-Lu fault. That event also reactivated and modified the trace of the Triassic sinistral Tan-Lu fault.

The Hua-Bei basin was formed by extension in a NNE direction at around ~150–130 Ma. At this time movement on EW structures ceased and NE trending structures were re-activated. The Hua-Bei Basin is a typical example of a basin system formed in a trans-tensional stress regime. We hypothesize that the change in the stress regime was caused by slab roll-back occurring on the Pacific subduction zone to the East. Retrograde motion of the subduction zone may have reduced the EW compressional stress sufficiently to trigger the gravitationally induced spreading of the thickened, unstable lithosphere of the North China block.

In our calculations we represent this change in boundary conditions by halting the northward movement of the southern boundary at $t/T=1.0$, setting $u_y=0$, but allowing it to move eastward by setting the x-component of traction T_x to represent a lithostatic condition on the eastern boundary. Both of these

changes are effected at a time that corresponds to a maximum convergent displacement of D at $x/D=6$ (the eastern side of the model). The lithostatic condition describes a boundary on which applied shear stress is zero and applied normal stress is equal to the lithostatic stress arising from a column of reference lithosphere that is unable to support significant deviatoric stress (Houseman and England, 1993). The lithostatic boundary moves outward only in response to gradients of stress or gravitational potential energy within the solution region. Traction components T_x and T_y on the lithostatic boundary are thus set so that the traction vector is normal to the boundary, and their magnitudes are proportional to the contrast in gravitational potential energy across the boundary. By subtracting out the lithostatic part of the stress field in the thin viscous sheet, the lithostatic condition becomes $T_x=T_y=0$.

In keeping with the idea that the lithosphere may move eastward in response to gravitationally driven extensional forces, we also modify the condition on the northern boundary, so that $u_y=0$ still, but we permit eastward movement by means of a frictional condition on the x-component,

$$T_x = -cu_x, \tag{10}$$

in which the friction coefficient c is set to a dimensionless value $c=0.25$ (linearly tapered to $c=0$ over the easternmost $2D$ length of the boundary). Thus, the eastward movement of the North China block is resisted by a frictional traction proportional to the displacement rate, representing the work that must be done to deform regions north of the boundary. The idea of a friction coefficient allows us to explore boundary conditions that are intermediate between the limiting cases of zero displacement ($c\rightarrow\infty$) and zero traction ($c=0$). We experimented with some different values of c and chose the value 0.25 as that which permitted a plausible amount of eastward extension, while ensuring that a trans-tensional stress environment is maintained. The value of c is tapered to zero at the northeastern corner so as to avoid the stress-singularity that appears there if traction is discontinuous. The western boundary ($x=0$) remains fixed, unchanged from stage 1 of the calculation.

Stage 2 of the calculation is stopped after an additional dimensionless time of 0.5, corresponding in dimensional terms to an additional period of 50 Myr.

2.4. Strength variation within the North China block

The North China region includes metamorphic basement rocks as old as the early Archean (>3800 Ma; Liu et al., 1992). Despite this ancient provenance, however, it has not behaved as a rigid block during these Mesozoic deformation episodes. As pointed out by Şengör and Natal'in (1996), it hardly deserves the title 'craton' if one considers its tectonic evolution during the late Precambrian, Paleozoic and Mesozoic. In contrast, the Ordos block embedded within the North China region (Fig. 1) is topographically elevated, and does appear to have behaved as a rigid block in which little deformation is evident. This relative rigidity may be explained by this block having a greater resistance to deformation, whether because this lithosphere is colder, dryer or has different composition.

We include also in our tectonic model (Fig. 3) a boundary that trends mainly northeastward, representing the contrast between the North China block and the subduction–accretion complexes of the Altaid and Manchuride belts to the north, described by Şengör and Natal'in (1996). A part of the Altaid region of Mongolia is represented in the northwest part of our tectonic model. The Altaid and North China regions have distinct tectonic histories, finally coming together in the Permian. The extension that affected the North China block in the Cretaceous did not apparently reach into the Altaid region. A simple hypothesis that might explain this contrast in behaviour is that the North China Block is weaker and more easily deformed than both Altaid-Mongolia and Ordos regions. The weaker region between Altaid-Mongolia and Ordos blocks will clearly be the locus of maxiumum deformation under a regional stress field. This region is identified with the modern day Yin Shan (Fig. 1).

We assume that this contrast in properties between the Ordos block, the North China region and the Altaid-Mongolia region can be interpreted in terms of a difference in the effective strength parameter of the regions defined in our simplified tectonic model (Fig. 3). Relative to the strength coefficient B that is used in the definition of the Argand number, we

arbitrarily specify the dimensionless strength coefficient of the Altaid-Mongolia region in the northwest to be 1, that of the stronger Ordos block to be $(2.0)^{1/n}$ (≈ 1.26 if $n=3$), and that of the weaker North China block to be $(0.2)^{1/n}$ (≈ 0.5848 if $n=3$). These strength contrasts are scaled relative to the value of n in order that the contrast in effective viscosity between the different regions is comparable for both values of $n=1$ and 3 that we use (England and Houseman, 1985; Neil and Houseman, 1997). We assume in these calculations that relative lithospheric strength variations are preserved during deformation. Although it is likely that lithospheric strength may decrease as it thickens, due to the greater thickness of crust, the deformation history is not sufficiently well constrained to justify a more complex model.

To facilitate the interpretation of our results, Lagrangean strain markers are displayed on the plots, to indicate relative displacement and internal deformation. The initial distribution of the circular strain makers is displayed in Fig. 3.

2.5. Gravitational potential energy and the Argand number

Deformation of the thin viscous sheet is driven partly by boundary stresses and partly by internal gradients of the gravitational potential energy. In the simplified formulation of England and McKenzie (1982), the gradients in potential energy are given by the term on the right hand side of Eq. (3). The Argand number, depending on the depth-integrated strength of the layer is difficult to constrain, but England and Houseman (1986) estimated that $Ar=1$ is appropriate for $n=3$. We therefore use $Ar=1$, and for comparison $Ar=4$, in the first stage of these numerical simulations (both for $n=1$ and for $n=3$).

With $Ar=1$, the first stage of deformation may result in relatively high degrees of lithospheric thickening, particularly when $n=3$. We therefore follow Houseman et al. (1981), England and Houseman (1989), Molnar et al. (1993), Houseman and Molnar (1997), and Molnar et al. (1998) in suggesting that convergent thickening on this scale is likely to be followed by lithospheric convective thinning, in which the lowermost part of the cold thickened lithosphere drips down into the mantle to be replaced by hot asthenosphere from below, producing rapid elevation and heat input into the overlying crust. When we invoke this mechanism we use the approximate formulation of England and Houseman (1989) to simulate the effect of this process on the thin sheet calculations. When lithospheric thickness caused by horizontal shortening has exceeded a threshold level, the Argand number is assumed to locally undergo a step-like increase, which represents the sudden large increase in lithospheric gravitational potential energy that would accompany the convective thinning event. We therefore specify for the $Ar=1$ experiments that, when the crust attains a thickness of 60 km (relative to the assumed initial thickness of 35 km), Ar is locally increased to 4. For comparison we also computed solutions for the cases when Ar is uniformly high ($Ar=4$) throughout the calculation.

If convective thinning does not occur, the Argand number may remain small or even become negative, as suggested by Fleitout and Froidevaux (1982). Negative Argand number is generally not possible however if the dense lithospheric root is removed (England and Houseman, 1989) as seems necessary to explain the subsequent stage of extension.

3. Results

We first describe the results from different numerical experiments with either $n=1$ or $n=3$, corresponding to Newtonian or non-Newtonian viscous constitutive relation, and either $Ar=1$ or $Ar=4$, corresponding to the two assumptions about gravitational potential energy discussed above. The solutions for these experiments (with initial geometry shown in Fig. 3) are shown as maps of crustal thickness (Figs. 4 and 5) and maps of vertical strain-rate (Figs. 6 and 7) for both $n=1$ (Figs. 4 and 6) and for $n=3$ (Figs. 5 and 7).

The left columns of Figs. 4–7 depict the solutions after the initial stage of N–S shortening. The right columns show the solutions after the second stage of E–W extension. In Figs. 4 and 5, the non-dimensional crustal thickness is shown. After the first stage of deformation, the whole North China block (the weakest region) has been thickened, yet the thickness of the stronger Ordos and Altaid-

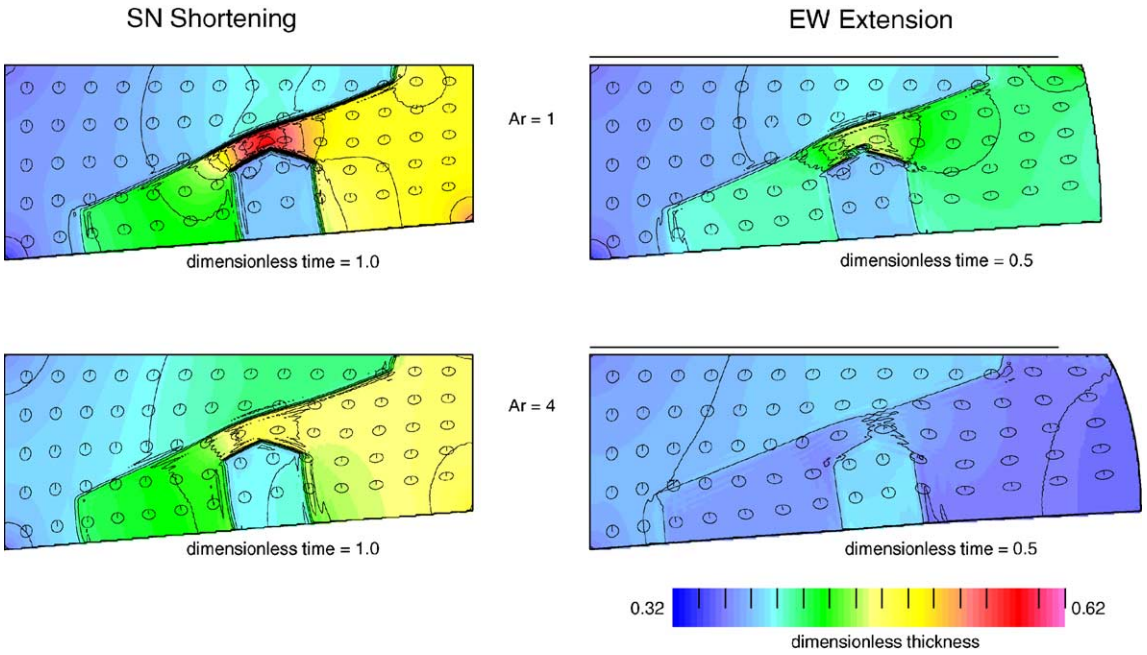

Fig. 4. Non-dimensional crustal thickness maps for two experiments with stress vs. strain-rate exponent $n=1$. Left column: After the period of N–S shortening (the first stage of deformation) when $t/T=1.0$; Right column: After the period of E–W extension (the second stage of deformation) and a further elapsed dimensionless time of 0.5. These experiments assume respectively: $Ar=1$ (top row) and $Ar=4$ (second row). Lithospheric thinning occurs here only for $Ar=1$ in a very localised region just north of the Ordos block. The solid lines above the maps on the right show the original length of the solution domain prior to extension.

Mongolia regions has changed little. The eastern part of the Hua-Bei plateau has been thickened by about 30% because convergence increases eastward due to the southern boundary condition. Crustal thickness in the Hua-Bei plateau has increased from the original 35 km to ~45 km, during the nominal 100 Myr convergence period.

The strain markers indicate the large degree of N–S shortening and E–W extension that occurs within the narrow relatively weak region immediately north of the Ordos block. When $n=1$ (Fig. 4), the crustal thickness builds up in the Yin Shan, between the Ordos block and the Altaid-Mongolia region. If $Ar=1$, crustal thickness reaches 60 km, limited by the onset of convective thinning and the local increase of Argand number, but if $Ar=4$ the thickness there reaches only about 46 km. When $n=3$ and $Ar=1$ (Fig. 5), the crustal thickening in the Yin Shan region reaches 60 km over a somewhat greater area. When $Ar=4$, however, for the non-Newtonian experiments, crustal thickening in this region still reaches about 56 km. Also evident in some of the experiments is a small region of intense crustal thickening in the SE corner of the model. This thickening is an artifact caused by the acute angle between eastern and southern boundaries, and has no tectonic relevance to our discussion of the North China block.

The distribution of crustal thickening after the first stage of deformation is generally similar for $n=1$ (Fig. 4) and for $n=3$ (Fig. 5) for either of the Argand number models, although crustal thickness is locally greater for $n=3$ than for $n=1$. In both cases the thickness of the Ordos and Altaid-Mongolia regions increases by only a few km, and thickness east of the Ordos block generally increases eastward to approximately 50 km during this period of prescribed convergence. The apparent near-equivalence between solutions for Newtonian and non-Newtonian viscosity arises presumably because the external boundary conditions during this first stage of the calculation require the same total strain, and the internal variation of effective lithospheric viscosities are similar. We will see, however, that significant

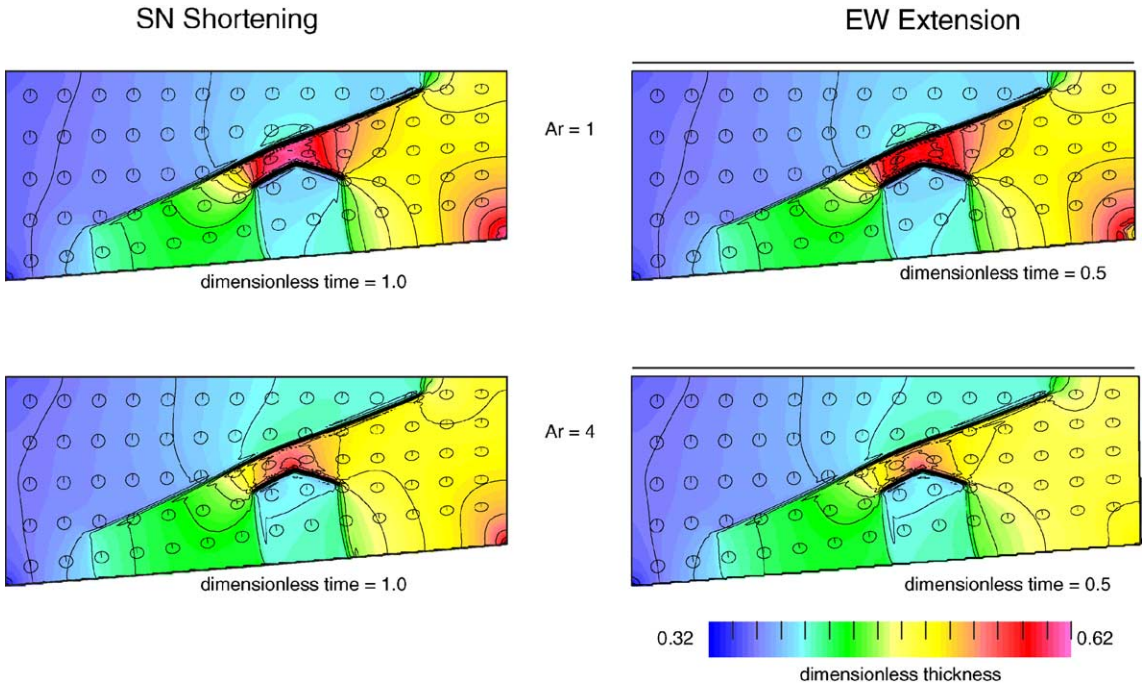

Fig. 5. Non-dimensional crustal thickness maps for two experiments with stress vs. strain-rate exponent $n=3$. These experiments assume respectively: $Ar=1$ (top row) and $Ar=4$ (second row), except that where crustal thickness exceeded 60 km in the former, lithospheric thinning was simulated by locally increasing Ar from 1 to 4. Left column: After the period of N–S shortening at $t/T=1.0$; Right column: After the period of E–W extension that constitutes the second stage of deformation. Solid lines above the maps on the right again show the original length of the solution domain.

differences develop between $n=1$ and $n=3$ in the second phase of deformation, as the E–W extension develops.

The vertical strain-rate, which is related to the rate of crustal thickening by Eq. (5), is generally positive everywhere during the first stage of deformation (left columns of Figs. 6 and 7) and shows a gradational increase eastward across each of the regions, with peak values of strain rate developing on the corners of the strong regions. Because crustal thickness (Figs. 4 and 5) effectively represents the time integral of the vertical strain-rate (Figs. 6 and 7) small contrasts in thickening rate develop with time into large contrasts in crustal thickness. For example, comparing two regions where the vertical strain rate differs by a factor of two, the crustal thickening factor of the more active region will be the square of that for the less active region after the same elapsed time.

For each of the second stage (extension) experiments, the initial state is taken from the crustal thickness distribution at the end of the first stage (convergence) experiments, as described earlier. The boundary conditions for the second stage calculations were also described earlier, and include the frictional northern boundary and the lithostatic eastern boundary. The Argand number assumption remains constant from first to second phase of deformation. The state of the lithosphere at the end of the second stage of deformation is shown in the right columns of Figs. 4–7.

For $n=1$ the extension of the thickened crust in the Hua-Bei region is indicated in the right column of Fig. 4, by the decreased crustal thickness and the strain markers that are stretched in the E–W direction. The relatively rigid Ordos block and Altaid-Mongolia region remain almost unchanged in crustal thickness. The orogenic Yin Shan region between Ordos and Altaid-Mongolia thins most as extension occurs during the second stage. Crustal thicknesses of about 46 km are still found in the Yin Shan region for $Ar=1$, but when $Ar=4$ the crustal thickness there almost

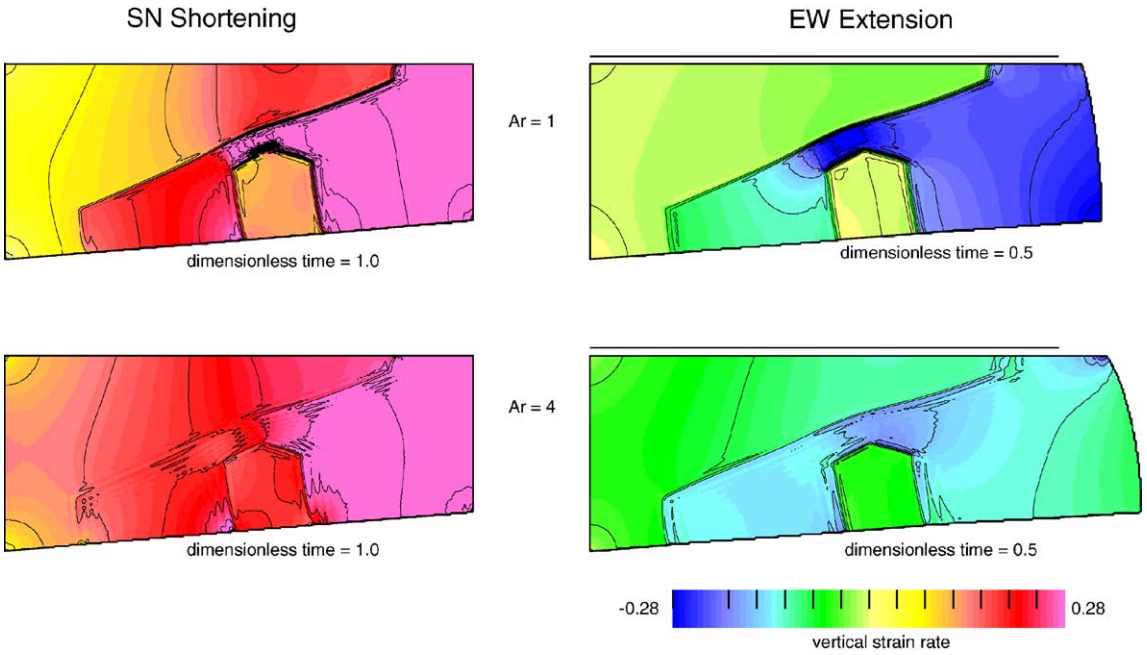

Fig. 6. Map of vertical strain rate ($\dot{\varepsilon}_{zz}$) for the $n=1$ experiments shown in Fig. 4. Strain-rates greater than zero imply thickening. For a dimensional time unit of 100 Myr, a dimensionless strain-rate of 1 represents a dimensional rate of 1% Myr^{-1}. Left column: strain-rates at end of the first stage of deformation ($t/T=1$); Right column: strain-rates at end of the second stage of deformation. Physical and computational parameters are as for Fig. 4.

returns to its original 35 km. The negative vertical strain rates for $n=1$ (Fig. 6, right column) indicate that crustal thinning continues to be active at the end of the experiment when $Ar=1$, whereas for $Ar=4$ extension occurred more rapidly and is essentially complete at the end of the time interval allowed for the second stage of deformation. For the $n=1$ experiments, the threshold for convective thinning is not reached at all (with $Ar=4$), or barely reached in a small region (with $Ar=1$), so convective thinning has little impact on these calculations.

For $n=3$ (Fig. 7, right column), we see that the vertical strain-rates at the end of the second stage of deformation are negative, but their amplitudes are small almost everywhere, and consequently the crustal thickness distribution (Fig. 5, right column) does not change much during the second stage of deformation, and the Hua-Bei region remains relatively thick, with crustal thicknesses on the order of 42–44 km to the west of the Ordos block, and 48–50 km to the east. Only in the Yin Shan orogenic zone does significant extension occur, because the threshold for convective thinning has been exceeded, and this only in the case where we initially assumed $Ar=1$. If $Ar=4$ crustal thickening is not sufficiently localised to trigger convective thinning, even for the $n=3$ experiments. Therefore, lithospheric convective thinning is most likely to be of significance in regard to the evolution of the Yin Shan orogenic belt, but is not necessarily implicated in the widespread extension that occurred in the eastern part of the Hua-Bei Basin.

Crustal thinning rates in the eastern Hua-Bei region during the second stage of the experiments are much less for $n=3$ than for $n=1$ because the combination of fixed traction boundary condition and non-Newtonian viscosity, with $Ar=4$ or less, does not drive gravitational collapse at a significant rate. In choosing parameter values for the above experiments we have been guided by previous lithospheric-scale tectonic models of the deformation in active regions (e.g., England and McKenzie, 1982; Houseman and England, 1996; Roberts and Houseman, 2001). We caution, however, that the relative stabilisation of these $n=3$ experiments might not be robust under other assumptions. The gravitational

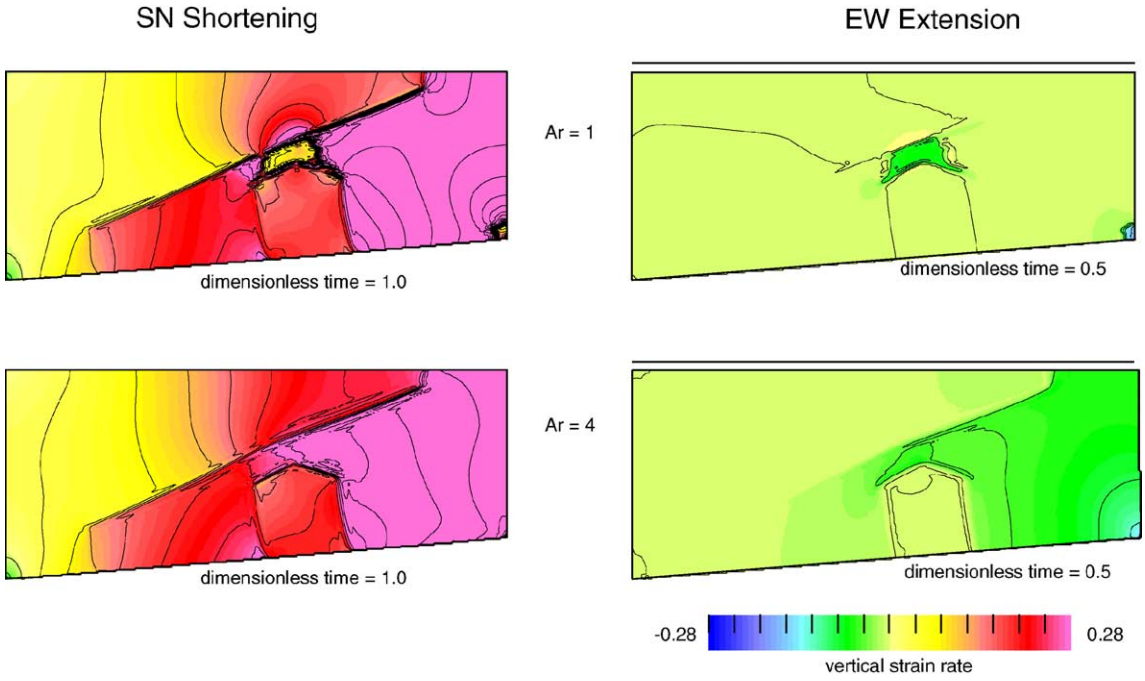

Fig. 7. Map of vertical strain rate ($\dot{\varepsilon}_{zz}$) for the $n=3$ experiments shown in Fig. 5, using the same physical and computational parameters. Interpretation of strain-rate units and colour scales is as shown in Fig. 6. Note that the strain-rate maps for $n=3$ and $n=1$ (Fig. 6) are similar during stage one of deformation, but differ qualitatively during stage two, in that extensional rates are less in the North China region for $n=3$, except where lithospheric thinning has caused a local increase in Argand number in the Yin Shan region between Ordos and Altaid-Mongolia Blocks.

collapse that occurs in the $n=1$ experiments only occurs because the assumed viscosity is relatively low. It might also be induced to occur in the $n=3$ experiments if: Ar were significantly greater than 4, or convective thinning were induced to occur at the relatively low thickening factors obtained after the first stage of the experiment, or extension were induced by boundary conditions, such as back-arc extension on a subduction zone to the East.

There is a trade-off between the effect of reducing the horizontal confining stress on the eastern boundary and increasing the vertical stress by a convective thinning event. For the above experiments we set the eastern boundary lithostatic stress to be in equilibrium with a continental column with crust of thickness 35 km. The extension depicted in the right columns of Figs. 4 and 6 is effectively limited by this assumption. Thinning of the crust in the Hua-Bei region to 30 km or less could result from further reducing the magnitude of the confining stress on that boundary, for either value of n.

4. Discussion

The relatively low amplitudes of free-air gravity anomalies in East China have been used to infer the approximately isostatic state of the lithosphere in this region. It is generally assumed that topography is compensated by variations in crustal thickness. The crustal thickness of the Ordos Plateau is inferred to be between 40 and 44 km. In the Hua-Bei basin to the east, the greatest depths to the Moho, approximately 36 km, occur on the edges of the basin, adjacent to the Taihang Shan (east of the Ordos block), the Yan Shan (on the north side of the Hua-Bei basin), the Tai Shan adjacent to the Tan-Lu fault in the east, and beneath the Da-Bie Shan in the south; In the centre of the Hua-Bei basin crustal thickness is variable, but typically around 32 km. The shallowest Moho, around 28 km, is in the north–east corner of the Hua-Bei basin on Bo-Hai Bay. Although there are small positive free-air anomalies (20–30 mgal) over the Bo-Hai Bay, the entire region in general is nearly in isostatic equilib-

rium (Ma et al., 1982). The gravity data therefore indicate that the depth to the Mohorovicic discontinuity is roughly 10–12 km shallower in the center of the Hua-Bei Basin than the neighbouring Ordos block.

Moho depths inferred from seismic studies are used to constrain and are generally consistent with those inferred from gravity. Crustal thickness is 40–45 km, under the Ordos block and Inner Mongolia to the north and west of the Hua-Bei Basin (Feng and Teng, 1983). The seismic evidence also implies that the crust beneath the central Hua-Bei Basin is significantly thinner than that in the surrounding regions. The *P*-wave velocities in the upper mantle beneath the Hua-Bei Basin are variable, but up to 3% higher than average in the eastern part of the basin, and beneath the Ordos block. Lower velocities are found in a north–south trending zone that coincides with a zone of high gravity gradient that follows the Taihang Shan across the Hua-Bei basin (Liu et al., 1990).

Heat flow measurements in the North China basin region are variable. Greater than average heat flows are found in the Bo-Hai Basin and the ShanXi Graben to the east of the zone of steep gravity gradient (Ye et al., 1985). These regions have been subject, however, to Tertiary tectonic activity, and these data therefore do not provide specific evidence about the evolution of the Hua-Bei basin during the Mesozoic. More relevant constraints are obtained from fission track analyses from the North China block. These data document three stages in the geothermal evolution of the lithosphere since the Triassic, with the temperature of the lithosphere gradually increasing during the early to middle Jurassic, followed by a thermotectonic event during the late Jurassic to early Late Cretaceous (140–130 Ma), and then cooling from the late Cretaceous (about 85 Ma) to the Quaternary (Sun et al., 1994). This thermotectonic event may be interpreted in the light of McKenzie's (1978) model of lithospheric extension and basin formation. Stretching of continental lithosphere causes thinning and up-welling of hot asthenosphere. The lithosphere then re-equilibrates by conduction, generally accompanied by slow cooling and subsidence. The Ordos basin by comparison has remained a stable platform with low heat flow throughout the Paleozoic, Mesozoic and Cenozoic.

The North China block has been intruded by Ordovician diamondiferious kimberlites and Cenozoic alkali basalts both containing mantle xenoliths. The early Paleozoic diamondiferious character of some of the kimberlite pipes, and the predominance of peridotitic type inclusions in diamonds, suggest that the early Paleozoic lithosphere was thick and stable to depth within the diamond stability field (i.e. ~200 km) with a very low thermal gradient <40 mW m^{-2} (Menzies et al., 1993). However, Cenozoic lithosphere (Neogene-Quaternary), revealed by basalt-borne mantle xenoliths as well as geophysical observations (Ma, 1987), was thin (<80 km) and Cenozoic lithospheric mantle was characterized by chemically fertile but isotopically depleted compositions in Sr and Nd (Griffin et al., 1998; Fan et al., 2000; Guo et al., 2001). These observations have been interpreted to suggest that the lithospheric mantle has been thinned beneath the North China block by as much as 100 km since the early Paleozoic (Menzies et al., 1993).

The late Mesozoic lithosphere of the Hua-Bei basin thus appears to be in a transitional state from thick cold lithosphere typical of the early Paleozoic to hot thin lithosphere that may be found in many tectonically active regions in the Cenozoic. The implied Archaean lithospheric keel was apparently preserved until the late Mesozoic, even through the Triassic continental collision between the North and South China blocks. The late Mesozoic mafic intrusives and coeval basaltic rocks thus are interpreted to have recorded the beginning of lithospheric thinning. The thinning mechanism is likely to have been complex, and the simple numerical experiments in the previous section represent only one plausible mechanism.

Our experiments with $n=3$ were unable to predict the present-day distribution of crustal thickness for the range of Argand numbers that we examined. With the non-Newtonian viscous constitutive law, the large stresses required to activate deformation at significant strain-rates are not available from buoyancy forces alone when $Ar \leq 4$. When the convergent driving force is removed, and the constraining boundary conditions relaxed, minor thinning occurred in the Hua-Bei basin, in these experiments, but the rates were too slow to result in significant crustal extension over the nominal 50 Myr period of the extension stage of the calculation (Fig. 7). The inability of the $n=3$ experiments to explain the

extensional stage of deformation may lie in our assumptions. In particular, we assumed that convective thinning would require a threshold crustal thickness of about 60 km. Where gravitational instability has been invoked in other settings, such as Tibet (England and Houseman, 1989), it has been inferred that a threshold crustal thickness of around 60 km must be reached before convective thinning occurs, in order to match present day observations (Molnar et al., 1993; Neil and Houseman, 1997). In the North China block, however, the geometrical constraints seem to require that if convective thinning has been widespread in the eastern part of the basin, then it was triggered at lower crustal thickening ratios, when crustal thickness had attained only 50 km perhaps, relative to the original 35 km thickness.

We found, however, for $n=1$, and Ar between 1 and 4, that our numerical simulations predict approximately the distribution of crustal thickness that is observed across the Hua-Bei basin and the Ordos block. While the $n=1$ simulations do not require the degree of lithospheric thinning that is inferred from geochemical studies of lithospheric xenoliths, neither do they necessarily exclude it. The difficulty of requiring convective thinning to be initiated over a broad area by relatively modest thickening factors remains, however. The inferred reduction of lithospheric thickness from the original 200 km to Quaternary thickness of around 80 km implied by the xenolith data (Menzies et al., 1993) might therefore be attributable to other effects, such as more recent hot asthenospheric up-welling, or mantle plume activity.

Although previous studies of the Tertiary India-Asia collision have suggested that a non-Newtonian viscosity is a better representation of the constitutive relation that describes the large-scale long-term deformation of the lithosphere in that region, it may well be that the tectonic evolution of the North China Block has occurred over greater time intervals and generally lower stress-levels. Lower stress levels could explain why the linear lithospheric constitutive relation used in Figs. 4 and 6 is more appropriate here.

This model does not explain the development of the Yan Shan fold and thrust belt which extends at least 1100 km eastward of the Yin Shan. These two fold belts are generally assumed to have a common tectonic history because of their current spatial aligment but an alternative explanation (Davis et al., 2001) has the Yan Shan develop as a continental margin orogen related to Pacific plate-North China plate interaction.

5. Conclusions

We have used the thin viscous sheet model to represent the tectonic processes occurring in the North China block during the Mesozoic. The history of convergent deformation of this region during the Triassic to late Jurassic, followed by extension in the late Jurassic to Cretaceous, places some constraints on the evolution and rheological properties of the lithosphere. The crust in the North China block was thickened in the Triassic and Jurassic by N–S shortening. A change in the regional stress field triggered wide-spread E–W extension in the Cretaceous. Simulations of the tectonic history using a two-stage model with a Newtonian depth-averaged constitutive relation, and Argand number >4 can explain much of the observed distribution of crustal thicknesses. Widespread thickening of the lithosphere in the North China Block by as much as 50% was followed by extension, which restored crustal thickness to around 35 km, or less, depending on the confining stress provided by the eastern boundary. This model does not require that the lithosphere was thinned much relative to its original pre-Mesozoic thickness. Gravitational instability of the thickened lithosphere is most likely to have occurred in the Yin Shan region. We also cannot rule out the possibility that some kind of convective thinning event caused a greater degree of lithospheric thinning prior to crustal extension, as is suggested by thermobarometric studies of xenoliths from Paleozoic and Cenozoic volcanic fields, but geometrical constraints would suggest that if such a convective thinning event did occur, then it occurred when crustal thickness of the region was perhaps only 50 km or less.

Extension occurred in the Hua-Bei region because the vertical stress field (directly proportional to the Argand number) was sufficiently greater than the E–W stress, which is determined by the static stress on the Eastern boundary. In our simulations,

we found that crustal extension in the eastern region causes the crust there to thin until its thickness approaches that of the reference column that defines the stress on the eastern boundary, provided that the lithosphere responds with a Newtonian viscosity ($n=1$) and an effective depth-averaged viscosity that yields Ar greater than about 4. It is clear, however that the same degree of extension might have resulted if a convective thinning event had first occurred beneath the North China lithosphere, and thus changed the relative balance between vertical and horizontal stress. The latter explanation is perhaps more consistent with the degree of lithospheric thinning implied by the xenolith studies. The tests of this model examined here cover only a small subset of possible parameter ranges, and therefore constitute only a preliminary exploration of this problem, and may serve as a guide for further investigation of the regional tectonics of the North China block.

Acknowledgements

This project is supported by Natural Science Fundation of China (no. 40230056) and the Guangzhou Institute of Geochemistry, Chinese Academy of Sciences (no. GIGCX-03-02 and 030513). We thank Kevin Furlong and two anonymous referees for their thoughtful comments on an earlier version of the manuscript.

References

Bird, P., Piper, K., 1980. Plane-stress finite element models of tectonic flow in southern California. Phys. Earth Planet. Inter. 21, 158–175.

Davis, G.A., Qian, X., Zheng, Y., Tong, H.-M., Yu, H., Wang, C., Gehrels, G.E., Shafiquallah, M., Fryxell, J., 1996. Mesozoic deformation and plutonism in the Yunmeng shan: a metamorphic core complex north of Beijing, China. In: Yin, A., Harrison, T.M. (Eds.), The Tectonic Evolution of Asia. Cambridge University Press, New York, pp. 253–280.

Davis, G.A., Zheng, Y.D., Wang, C., Darby, B.J., Zhang, C.H., Gehrels, G., 2001. Mesozoic tectonic evolution of the Yanshan fold and thrust belt, with emphasis on Hebei and Liaoning Provinces, northern China. In: Hendrix, M.S., Davis, G.A. (Eds.), Paleozoic and Mesozoic Tectonic Evolution of Central Asia: From Continental Assembly to Intracontinental Deformation, Memoir Geological Society of America, vol. 194. Geological Society of America, Boulder, Colorado, pp. 171–197.

England, P.C., Houseman, G.A., 1985. Role of lithospheric strength heterogeneities in the tectonics of Tibet and neighboring regions. Nature 315, 297–301.

England, P., Houseman, G., 1986. Finite strain calculations of continental deformation II: comparison with the India-Asia collision zone. J. Geophys. Res. 91, 3664–3676.

England, P.C., Houseman, G.A., 1989. Extension during continental convergence, with application to the Tibetan plateau. J. Geophys. Res. 94, 17561–17579.

England, P.C., McKenzie, D.P., 1982. A thin viscous sheet model for continental deformation. Geophys. J. R. Astron. Soc. 70, 295–321 (correction: 73, 523–532, 1983).

England, P.C., Houseman, G.A., Sonder, L., 1985. Length scales for continental deformation in convergent, divergent, and strike-slip environments: analytical and approximate solutions for a thin viscous sheet model. J. Geophys. Res. 90, 3551–3557.

Fan, W.M., Zhang, H.F., Baker, J., Jarvis, K.E., Mason, P.R.D., Menzies, M.A., 2000. On and off the North China Craton: where is the archaean keel? J. Petrol. 41, 933–950.

Feng, C.-C., Teng, T.-L., 1983. Three-dimensional crust and upper mantle structure of the Eurasian continent. J. Geophys. Res. 88, 2261–2272.

Fleitout, L., Froidevaux, C., 1982. Tectonics and topography for a lithosphere containing density heterogeneities. Tectonics 1, 21–56.

Griffin, W.L., Zhang, A., O'Reilly, S.Y., Ryan, C.G., 1998. Phanerozoic evolution of the lithosphere beneath the Sino-Korean craton. In: Flower, M.F.J., Chung, S.-L., Lo, C.-H., Lee, T.-Y. (Eds.), Mantle Dynamics and Plate Interactions in East Asia, American Geophysical Union Geodynamics Series, vol. 27, pp. 107–126.

Guo, F., Fan, W.-M., Wang, Y.-J., Lin, G., 2001. Late Mesozoic mafic intrusive complexes in North China block: constraints on the nature of subcontinental lithospheric mantle. Phys. Chem. Earth, Part A Solid Earth Geod. 26, 771–795.

Guo, F., Fan, W.-M., Wang, Y.-J., Lin, G., 2003. Geochemistry of late Mesozoic mafic magmatism in west Shandong province, eastern China: characterizing the lost lithospheric mantle beneath the North China block. Geochem. J. 37, 63–77.

Hacker, B.R., Ratschbacher, L., Webb, L., McWilliams, M.O., Ireland, T., Calvert, A., Dong, S.W., Wenk, H.R., Chateigner, D., 2000. Exhumation of ultrahigh-pressure continental crust in east central China: late Triassic–Early Jurassic tectonic unroofing. J. Geophys. Res. 105, 13339–13364.

Houseman, G., 1996. From mountains to basin. Nature 379, 771–772.

Houseman, G.A., England, P., 1986a. A dynamical model of lithosphere extension and sedimentary basin formation. J. Geophys. Res. 91, 719–729.

Houseman, G.A., England, P., 1986b. Finite strain calculations of continental deformation: 1. Method and general results for convergent zones. J. Geophys. Res. 91, 3651–3663.

Houseman, G.A., England, P., 1993. Crustal thickening versus lateral expulsion in the India-Asian continental collision. J. Geophys. Res. 98, 12233–12249.

Houseman, G.A., England, P.C., 1996. A lithospheric thickening model for the Indo-Asian collisionr. In: Yin, A., Harrison, T.M. (Eds.), The Tectonic Evolution of Asia. Cambridge University Press, New York, pp. 3–17.

Houseman, G., Molnar, P., 1997. Gravitational (Rayleigh-Taylor) instability of a layer with non-linear viscosity and convective thinning of continental lithosphere. Geophys. J. Int. 128, 125–150.

Houseman, G.A., McKenzie, D.P., Molnar, P., 1981. Convective instability of a thickened boundary layer and its relevance for the thermal evolution of continental convergent belts. J. Geophys. Res. 86, 6115–6132.

Karato, S.-I., Paterson, M.S., Fitzgerald, J.D., 1986. Rheology of synthetic olivine aggregates; influence of grain size and water. J. Geophys. Res. 91, 8151–8176.

Li, S.G., Xiao, Y.L., Liou, D.L., Chen, Y.Z., Ge, N.J., Zhang, Z.Q., Sun, S.S., Cong, B.L., Zhang, R.Y., Hart, S.R., Wang, S.S., 1993. Collision of the North China and Yangtze blocks and formation of coesite-bearing eclogites: timing and process. Chem. Geol. 109, 89–111.

Liu, F.T., Wu, H., Liu, J.H., Hu, G., Li, Q., Qu, K.X., 1990. 3-D velocity images beneath the Chinese continent and adjacent regions. Geophys. J. Int. 101, 379–394.

Liu, D.Y., Nutman, A.P., Compston, W., Wu, J.S., Shen, Q.H., 1992. Remnants of 3800 Ma crust in the Chinese part of the Sino-Korean craton. Geology 20, 339–342.

Liu, S.F., Heller, P.L., Zhang, G.W., 2003. Mesozoic basin development and tectonic evolution of the Dabieshan orogenic belt, central China. Tectonics 22 (4), 1038. doi:10.1029/2002TC001390.

Ma, X.Y., 1987. Lithospheric Dynamics Map of China and Adjacent Seas and Explanatory Notes (scale 1:4,000,000). Geological Publishing House, Beijing.

Ma, X., Deng, Q., Wang, Y., Liu, H., 1982. Cenozoic graben systems in North China. Z. Geomorphol. 42, 99–116.

McKenzie, D., 1978. Some remarks on the development of sedimentary basins. Earth Planet. Sci. Lett. 40, 25–32.

Menzies, M.A., Xu, Y., 1998. Geodynamics of the North China craton. In: Flower, M.F.J., Chung, S.-L., Lo, C.-H., Lee, T.-Y. (Eds.), Mantle Dynamics and Plate Interactions in East Asia, American Geophysical Union Geodynamics Series, vol. 27, pp. 155–165.

Menzies, M.A., Zhang, M., Fan, W., 1993. Palaeozoic and Cenozoic lithoprobes and the loss of >120 km of Archaean lithosphere, Sino-Korean Craton, China. In: Pritchard, H.M., Alabaster, T., Harris, N.B.W., Neary, C.R. (Eds.), Magmatic Processes and Plate Tectonics, Special Publication Geological Society London, vol. 76. Geological Society of London, London, pp. 71–81.

Molnar, P., England, P., Martinod, J., 1993. Mantle dynamics, the uplift of the Tibetan Plateau, and the Indian monsoon. Rev. Geophys. 31, 357–396.

Molnar, P., Houseman, G.A., Conrad, C.P., 1998. Rayleigh-Taylor instability and convective thinning of mechanically thickened lithosphere: effects of non-linear viscosity decreasing exponentially with depth and of horizontal shortening of the layer. Geophys. J. Int. 133, 568–584.

Neil, E.A., Houseman, G.A., 1997. Geodynamics of the Tarim Basin and the Tian Shan in central Asia. Tectonics 16, 571–584.

Ratschbacher, L., Hacker, B.R., Webb, L., McWilliams, M.O., Ireland, T., Calvert, A., Dong, S.W., Chateigner, D., Wenk, H.R., 2000. Exhumation of ultrahigh-pressure continental crust in east central China: Cretaceous and Cenozoic unroofing and Tan-Lu fault. J. Geophys. Res. 105, 13303–13338.

Roberts, E.A., 2001. Geodynamics of central Australia during the intraplate Alice Springs Orogeny; thin viscous sheet models. In: Miller, J.A., Holdsworth, R.E., Buick, I.S., Hand, M. (Eds.), Continental Reactivation and Reworking, Geol. Soc. Spec. Publ., vol. 184, pp. 139–164.

Şengör, A.M.C., Natal'in, B.A., 1996. Paleotectonics of Asia: fragments of a synthesis. In: Yin, A., Harrison, T.M. (Eds.), The Tectonic Evolution of Asia. Cambridge University Press, New York, pp. 486–640.

Sun, S., Wang, L., Lin, G., Liu, S., Chen, J., Xiao, B., Wang, J., 1994. Geothermal evolution and tectono-sedimentation of the North China crustoblock and their effects on the formation of oil/gas pools. Geotecton. Metallogen. 14, 51–57.

Wang, Q.C., Zhai, M.G., Cong, B.L., 1996. Regional geology. In: Cong, B.L., (Eds), Ultrahigh-pressure metamorphic rocks in the Dabieshan-Sulu region of China. Science Press, Beijing and Kluwer Acad. Pub., Dordrecht, pp. 8–26.

Xu, J., Ma, G., Zhu, G., Tong, W.X., Gui, K.R., Liu, Q., 1987. Formation and evolution of the Tancheng-Lujiang wrench fault system: a major shear system to the northwest of the Pacific Ocean. Tectonophysics 134, 273–310.

Ye, H., Shedlock, K.M., Hellinger, S.J., Sclater, J.G., 1985. The North China basin: an example of a Cenozoic rifted intraplate basin. Tectonics 4, 153–169.

Yin, A., Nie, S.Y., 1993. An indentation model for the North and South China collision and the development of the Tan-Lu and Honam fault systems, eastern Asia. Tectonics 12, 801–813.

Yin, A., Nie, S.Y., 1996. A Phanerozoic palinspastic reconstruction of China and its neighboring regions. In: Yin, A., Harrison, T.M. (Eds.), The Tectonic Evolution of Asia. Cambridge University Press, New York, pp. 442–485.

Zheng, J.P., O'Reilly, S.Y., Griffin, W.L., Lu, F., Zhang, M., Pearson, N.J., 2001. Relict refractory mantle beneath the eastern North China block: significance for lithosphere evolution. Lithos 57, 43–66.

Zheng, Y.F., Wang, Z.R., Li, S.G., Zhao, Z.F., 2002. Oxygen isotope equilibrium between eclogite minerals and its constraints on mineral Sm–Nd chronometer. Geochim. Cosmochim. Acta 66, 625–634.

Zhou, D., Graham, S.A., 1996. The Songpan–Ganzi complex of the western Qinling Shan as a Triassic remnant ocean basin. In: Yin, A., Harrison, T.M. (Eds.), The Tectonic Evolution of Asia. Cambridge University Press, New York.

Zhu, G., Song, C.Z., Wang, D.X., Liu, G.S., Xu, J.W., 2001. $^{40}Ar/^{39}Ar$ chronology of the strike-slip ages of the Tan-Lu fault zone and its geological significance. Sci. China, Ser. D: Earth Sci. 31, 250–256.